Analysis of the ‘angulin’ proteins LSR, ILDR1 and ILDR2 – tricellulin recruitment, epithelial barrier function and implication in deafness pathogenesis

Tomohito Higashi, Shinsaku Tokuda, Shin-ichiro Kitajiri, Sayuri Masuda, Hiroki Nakamura, Yukako Oda and Mikio Furuse

Journal of Cell Science 126, 3797

doi: 10.1242/jcs.138271

There was an error published in *J. Cell Sci.* **126**, 966-977.

There are mistakes in the notation of a mutant protein. All instances of R89Q (including in the figures) should in fact be R97Q.

The authors apologise for this mistake.

Analysis of the 'angulin' proteins LSR, ILDR1 and ILDR2 – tricellulin recruitment, epithelial barrier function and implication in deafness pathogenesis

Tomohito Higashi[1], Shinsaku Tokuda[1], Shin-ichiro Kitajiri[2], Sayuri Masuda[1], Hiroki Nakamura[1], Yukako Oda[1] and Mikio Furuse[1,*]

[1]Division of Cell Biology, Department of Physiology and Cell Biology, Kobe University Graduate School of Medicine, Kobe, 650-0017, Japan
[2]Department of Otolaryngology, Head and Neck Surgery, Graduate School of Medicine, Kyoto University, Kyoto, 606-8507, Japan
*Author for correspondence (furuse@med.kobe-u.ac.jp).

Accepted 15 November 2012
Journal of Cell Science 126, 966–977

doi: 10.1242/jcs.116442

Summary

Tricellular tight junctions (tTJs) seal the extracellular space at tricellular contacts (TCs), where the corners of three epithelial cells meet. To date, the transmembrane proteins tricellulin and lipolysis-stimulated lipoprotein receptor (LSR) are known to be molecular components of tTJs. LSR recruits tricellulin to tTJs, and both proteins are required for the full barrier function of epithelial cellular sheets. In the present study, we show that two LSR-related proteins, immunoglobulin-like domain-containing receptor (ILDR) 1 and ILDR2, are also localized at TCs and recruit tricellulin. At least one of LSR, ILDR1 and ILDR2 was expressed in most of the epithelial tissues in mice. The expressions of LSR, ILDR1 and ILDR2 were generally complementary to each other, although LSR and ILDR1 were co-expressed in some epithelia. ILDR1 was required for the establishment of a strong barrier of the epithelium, similar to LSR, when introduced into cultured epithelial cells, whereas ILDR2 provided a much weaker barrier. We further analyzed human ILDR1, mutations in which cause a familial deafness, DFNB42, and found that most DFNB42-associated ILDR1 mutant proteins were defective in recruitment of tricellulin. We also found that tricellulin mutant proteins associated with another familial deafness, DFNB49, were not recruited to TCs by ILDR1. These findings show the heterogeneity of the molecular organization of tTJs in terms of the content of LSR, ILDR1 or ILDR2, and suggest that ILDR1-mediated recruitment of tricellulin to TCs is required for hearing. Given their common localization at epithelial cell corners and recruitment of tricellulin, we propose to designate LSR, ILDR1 and ILDR2 as angulin family proteins.

Key words: Tricellular tight junction, Tricellular contacts, Epithelial barrier, Tricellulin, LSR, ILDR1, ILDR2, Deafness

Introduction

Tight junctions (TJs) play crucial roles in epithelial barrier function by regulating solute permeability through the paracellular pathway of transport (Anderson and Van Itallie, 2009; Schneeberger and Lynch, 2004). On transmission electron microscopy, TJs are visualized as focal contacts of the plasma membranes of adjacent cells to eliminate extracellular spaces (Farquhar and Palade, 1963). On freeze-fracture electron microscopy, TJs appear as a set of anastomosing intramembranous strands (TJ strands) (Staehelin et al., 1969). A belt of TJs surrounds each cell, and thereby a honeycomb-like pattern of TJs seals the whole intercellular space within the cellular sheets. The tetra-membrane-spanning proteins of the claudin family are the major components of TJ strands and are directly involved in the barrier property of TJs (Anderson and Van Itallie, 2009; Angelow et al., 2008; Furuse and Tsukita, 2006).

Within an epithelial cellular sheet, the paracellular pathway can be spatially divided into two routes: one between two adjacent cells and one at tricellular contacts (TCs), where the vertices of three or more cells meet. Freeze-fracture electron microscopy of TCs revealed specialized structures of TJs, named tricellular tight junctions (tTJs) (Friend and Gilula, 1972; Ikenouchi et al., 2005; Staehelin, 1973; Wade and Karnovsky, 1974; Walker et al., 1985). At TCs, the most apical elements of the TJ strands from both sides join and turn to extend in the basal direction, attaching to one another, to form tTJs. Thus, there are three sealing elements closely attached to each other to form a so-called 'central tube' structure in the extracellular space at TCs (Staehelin, 1973). It has been assumed that the narrow central tube of tTJs is responsible for the paracellular barrier function at TCs. Despite their potential roles in epithelial barrier function, TCs have not attracted much attention until the recent identification of their molecular components.

At present, tricellulin and lipolysis-stimulated lipoprotein receptor (LSR) have been identified as protein components of tTJs (Ikenouchi et al., 2005; Masuda et al., 2011). Tricellulin has four transmembrane domains and shares structural similarity with occludin, a TJ-associated membrane protein. In tricellulin-knockdown epithelial cells, transepithelial electrical resistance (TER) was decreased and the permeability of macromolecules was increased with impairment of tTJ formation (Ikenouchi et al., 2005). Exogenous expression of tricellulin at tTJs in MDCK II cells decreased the permeability of macromolecules without altering the ion permeability (Krug et al., 2009). Thus, tricellulin is required for maintenance of the tTJ barrier function. Moreover, tricellulin was reported to be the causative gene for a familial nonsyndromic deafness, DFNB49 (MIM 610153) (Chishti et al.,

Journal of Cell Science

2008; Riazuddin et al., 2006). LSR is a type I transmembrane protein that was recently identified as a tTJ-localizing protein by localization-based expression cloning (Masuda et al., 2011). LSR was originally identified as a lipoprotein receptor (Yen et al., 1999). LSR-knockdown EpH4 cells exhibited diffuse localization of tricellulin along the lateral plasma membrane, indicating that LSR is required for the localization of tricellulin at tTJs. The TER of LSR-knockdown cells was decreased compared with normal cells, suggesting that LSR maintains epithelial barrier function by recruiting tricellulin to tTJs (Masuda et al., 2011).

The structural proteins of cell–cell junctions often have homologous siblings and comprise protein families, which create functional diversity of cell–cell junctions or compensate their roles with one another. Tricellulin is one of three members of the TJ-associated MARVEL protein (TAMP) family (Raleigh et al., 2010). The other two members of this family, occludin and MARVEL domain-containing 3 (marveld3), were reported to be located at bicellular TJs (bTJs), indicating that among the TAMP family members only tricellulin is specific to tTJs (Raleigh et al., 2010; Steed et al., 2009). On the other hand, LSR has two closely related proteins encoded by the mammalian genome: immunoglobulin-like domain-containing receptor (ILDR) 1 and ILDR2. ILDR1 was originally identified as a protein expressed in lymphoma cells (Hauge et al., 2004). Recently, it has been revealed that *ILDR1* is the causative gene for a familial nonsyndromic deafness, DFNB42 (MIM 609646) (Borck et al., 2011). ILDR2 was reported to be a candidate modifier of susceptibility to type 2 diabetes (Dokmanovic-Chouinard et al., 2008). However, the functions of ILDR1 and ILDR2 have not yet been clarified at the cell biological level.

In the present study, we investigate whether ILDR1 and ILDR2 share similar functions to LSR in terms of tTJs. We show that ILDR1 and ILDR2 are localized to TCs in epithelial cells and recruit tricellulin to TCs, and that ILDR1 is responsible for the full barrier function of epithelial cellular sheets. Furthermore, we analyze the functions of the protein products of the mutated human genes encoding ILDR1 and tricellulin observed in the familial nonsyndromic deafnesses DFNB42 and DFNB49, respectively.

Results

Localization of ILDR1 and ILDR2 at TCs

We previously showed that LSR is localized at TCs in various epithelial tissues in mice and recruits tricellulin to TCs in the mammary epithelial cell line EpH4 (Masuda et al., 2011). However, during localization studies using immunofluorescence microscopy, we noticed that LSR expression was not detected in some tissues despite their concentration of tricellulin in TCs. In the colon, for example, LSR was only expressed in the lower portion of crypts, whereas tricellulin was concentrated at TCs throughout the entire crypts (Fig. 1A). Therefore, we speculated that some protein(s) may substitute for LSR in the recruitment of tricellulin to TCs in the regions where LSR is absent, such as the upper portion of crypts in the colon. As strong candidates, we examined the LSR-related proteins.

LSR has two homologous genes, *Ildr1* and *Ildr2*, in the mouse genome (Fig. 1B). Since all three genes have multiple splicing isoforms (supplementary material Fig. S1A), we chose one isoform for each gene based on the abundance in the expressed sequence tag (EST) database. Specifically, we evaluated mouse ILDR1 isoform 1, ILDR2 isoform 4 and LSR isoform 2, whose expressions in epithelial tissues were confirmed by reverse transcriptase–polymerase chain reaction (RT–PCR) (supplementary material Fig. S1B). These three proteins are type-I transmembrane proteins with an extracellular Ig-like domain and a long cytoplasmic tail. Their C-termini end equally in three hydrophobic amino acids, Leu-Val-Val (LSR), Val-Val-Ile (ILDR1) and Leu-Val-Val (ILDR2), which might be putative PDZ domain-binding motifs (Songyang et al., 1997). The three proteins share ~30% amino acid identity (Fig. 1B). A bootstrap analysis revealed that these proteins are evolutionarily conserved among vertebrates (supplementary material Fig. S2).

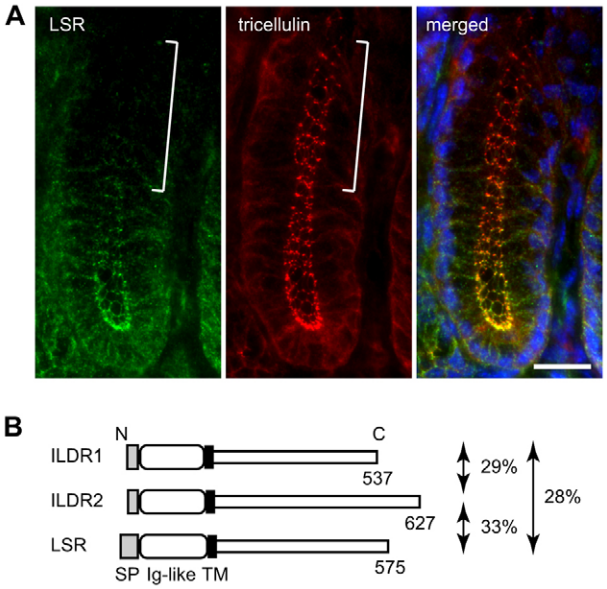

Fig. 1. Lack of LSR expression at TCs in mouse colon epithelial cells. (**A**) Double immunofluorescence staining of a frozen section of the mouse colon using anti-LSR pAb (green) and anti-tricellulin mAb (red). The merged image is shown with DAPI staining (blue) to visualize the nuclei. Note that LSR is not expressed in the upper region of the crypt (white bracket), whereas tricellulin is expressed and concentrated at the TCs in all epithelial cells of the crypt. Scale bar: 10 µm. (**B**) Schematic representation of the primary structures of the mouse ILDR1, ILDR2 and LSR proteins. All three proteins have a signal peptide (SP), an extracellular immunoglobulin-like domain (Ig-like), a single transmembrane domain (TM) and a long cytoplasmic tail. The amino acid identities among the three proteins are indicated.

Expression of ILDR1 and ILDR2 in mouse tissues

To examine the expression of the endogenous ILDR1 and ILDR2 proteins *in vivo*, we produced rabbit polyclonal antibodies (pAbs) against the cytoplasmic domain of mouse ILDR1 [amino acids (aa) 259–537] and that of mouse ILDR2 (aa 384–627). Among NIH/3T3 cells transiently expressing haemagglutinin (HA)-tagged ILDR1, ILDR2 or LSR (ILDR1–HA, ILDR2–HA or LSR–HA, respectively), each of the antibodies produced in the present study and the previously reported anti-LSR antibody recognized only the cells expressing the corresponding protein in immunofluorescence staining (supplementary material Fig. S3A–D). Furthermore, the addition of each corresponding immunogen abolished the staining (supplementary material Fig. S3E,F). From these results, we concluded that the antibodies against ILDR1, ILDR2 and LSR were specific for their targets, with no cross-reactivity towards the other proteins. The anti-ILDR1, anti-ILDR2 and anti-LSR antibodies were expected to recognize ILDR1 isoforms 1–3, ILDR2 isoforms 1–5 and LSR isoforms 1–3, respectively, because

these isoforms contain the corresponding epitopes (supplementary material Fig. S1A).

Next, we investigated the expressions and subcellular localizations of ILDR1, ILDR2 and LSR by immunofluorescence staining of frozen sections of various mouse tissues. In the upper portion of the crypts, where LSR was absent (Fig. 1A), ILDR1 expression was clearly detected at the TCs of epithelial cells (Fig. 2A). ILDR1 was also expressed and localized at TCs in a broad range of epithelial tissues, including the bladder, salivary gland, olfactory epithelium and kidney (Fig. 2B–E). The expression area of ILDR1 was generally complementary to that of LSR, although ILDR1 and LSR were co-expressed in some epithelia (supplementary material Table S1). ILDR2 was expressed at TCs in the epithelial tissues covering neural tissues, including the retinal pigment epithelium, perineurium and choroid plexus (Fig. 2F–H). The expression of ILDR1, ILDR2 or LSR (supplementary material Table S1) and tricellulin (data not shown) was detected in almost all types of epithelia. In some tissues, significant bicellular localization of ILDR1 or ILDR2 was also observed (Fig. 2F). To further examine the precise localization of the ILDR1 protein, we performed immunoelectron microscopy of the olfactory epithelium using the anti-ILDR1 pAb. As shown in Fig. 2I, ILDR1 signals were detected in close proximity to the plasma membrane of TCs, confirming our observations using immunofluorescence microscopy. These findings indicate that ILDR1 and ILDR2, in addition to LSR, are localized at the TCs of epithelial cells *in vivo* and that at least one of these three proteins is expressed in each epithelium. Although it is reasonable to speculate that ILDR1 and ILDR2 are located to tTJs by analogy with LSR (Masuda et al., 2011), we could not confirm their localizations at tTJs because our antibodies against these proteins did not work in immunoreplica electron microscopy (data not shown).

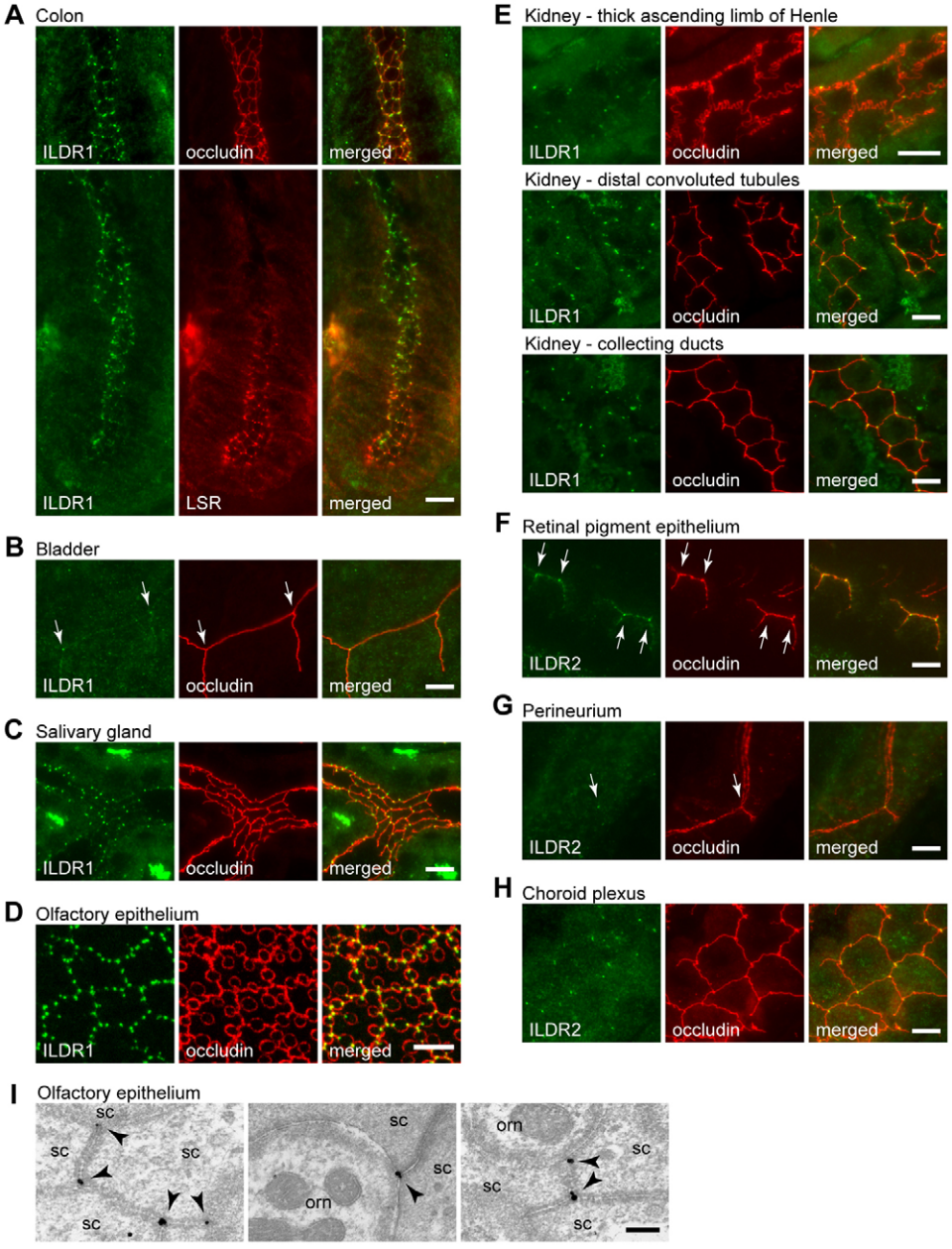

Fig. 2. Expression and subcellular localization of endogenous ILDR1 and ILDR2. (**A–H**) Immunofluorescence microscopy of ILDR1 and ILDR2 in mouse epithelial tissues. Frozen sections of mouse tissues were stained with anti-ILDR1 pAb (green) and anti-occludin mAb (red) (A, upper panels, and B–E), anti-ILDR1 pAb (green) and anti-LSR mAb (red) (A, lower panels) or anti-ILDR2 pAb (green) and anti-occludin mAb (red) (F–H). White arrows indicate TCs. (**I**) Immunoelectron microscopy of the olfactory epithelium with anti-ILDR1 pAb. Black arrowheads indicate ILDR1 signals located at TCs. orn, olfactory receptor neuron; sc, supporting cell. Scale bars: 10 μm (A–C,E–H); 5 μm (D); 200 nm (I).

Recruitment of tricellulin to TCs by ILDR1 and ILDR2

Next, to examine whether ILDR1 and ILDR2 recruit tricellulin to TCs, similar to the case for LSR, we expressed FLAG-tagged ILDR1 (ILDR1–FLAG) and ILDR2 (ILDR2–FLAG) in LSR-knockdown EpH4 cells (LSR-kd cells). In LSR-kd cells, the expression of ILDR1 or ILDR2 was negligible by immunofluorescence staining (supplementary material Fig. S4B) in addition to semi-quantitative RT–PCR (supplementary material Fig. S4C), and tricellulin was diffusely located to the lateral membrane (supplementary material Fig. S4B). When a small hairpin RNA (shRNA)-resistant FLAG-tagged LSR (LSR–FLAG) was expressed in LSR-kd cells as a positive control, LSR–FLAG was localized at TCs and the concentration of tricellulin at TCs was restored (Fig. 3B), consistent with our previous report (Masuda et al., 2011). When ILDR1–FLAG or ILDR2–FLAG was expressed instead of LSR–FLAG, they were also localized at TCs and recruited tricellulin (Fig. 3B). The expression levels of occludin, tricellulin, claudin-3 and zonula occludens 1 (ZO-1) in these cells were not changed compared with parental EpH4 cells (Fig. 3A). These findings indicate that the expression of any one of LSR, ILDR1 and ILDR2 is sufficient for the recruitment of tricellulin to TCs in epithelial cells.

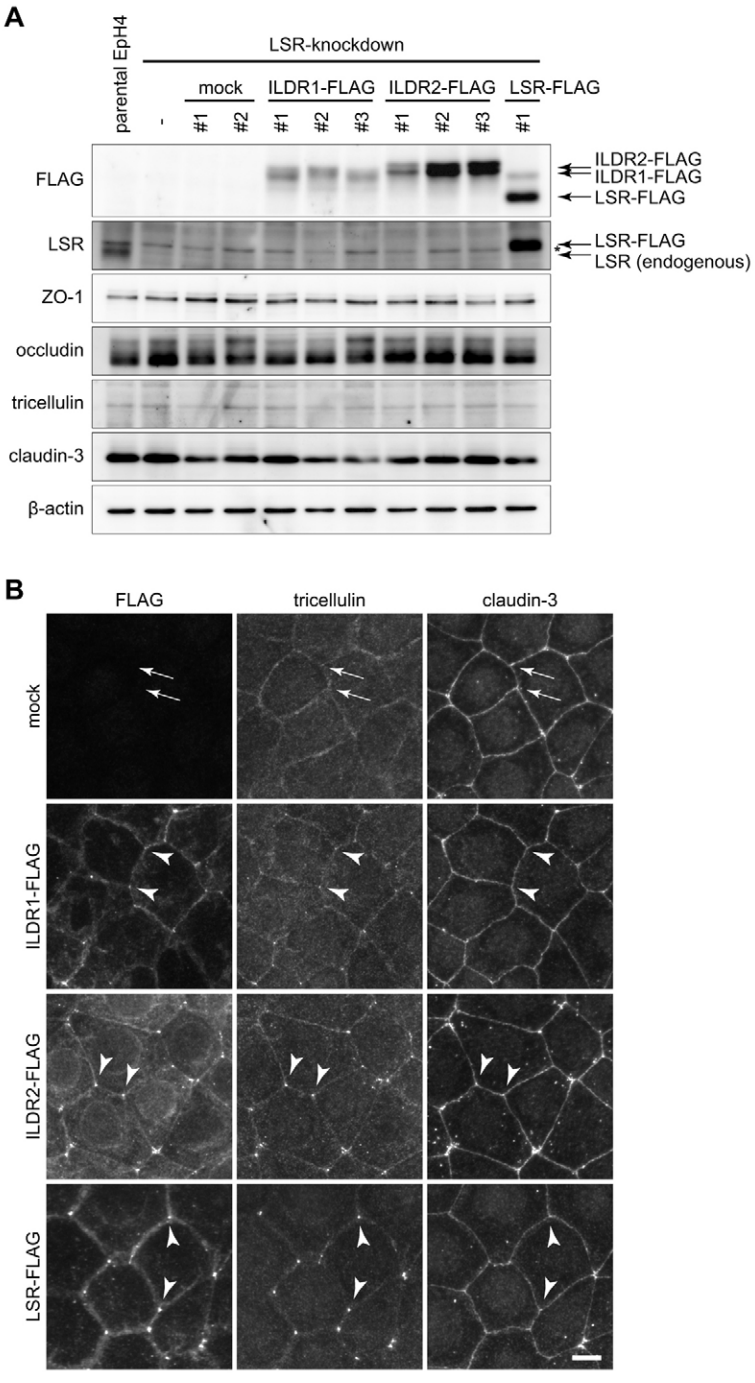

Fig. 3. Recruitment of tricellulin by ILDR1 and ILDR2. (**A**,**B**) Stable clones of LSR-kd cells expressing mock FLAG vector, ILDR1–FLAG, ILDR2–FLAG or LSR–FLAG were subjected to immunoblotting with anti-FLAG mAb, anti-LSR pAb, anti-ZO-1 mAb, anti-occludin pAb, anti-tricellulin mAb, anti-claudin-3 pAb or anti-β-actin mAb (A) or immunostained with anti-FLAG mAb, anti-tricellulin mAb and anti-claudin-3 pAb (B). The arrowheads and arrows in B indicate TCs with and without tricellulin localization, respectively. Scale bar: 10 μm.

Interactions of ILDR1 and ILDR2 with tricellulin

We previously showed that the C-terminal cytoplasmic domain of tricellulin interacts with LSR in living cells (Masuda et al., 2011). It is also of interest to determine whether ILDR1 and ILDR2 interact with tricellulin. Thus, we examined the binding of LSR, ILDR1 and ILDR2 to the TAMP family members, including occludin, tricellulin and marveld3. HEK293T cells were transiently co-transfected with FLAG-tagged occludin (FLAG–occludin), tricellulin (FLAG–tricellulin), marveld3 variant 1 (FLAG–marveld3-1) or marveld3 variant 2 (FLAG–marveld3-2) together with ILDR1–HA, ILDR2–HA or LSR–HA, followed by immunoprecipitation with an anti-FLAG monoclonal antibody (mAb). As a negative control for FLAG–tricellulin, FLAG-tagged CD9 (FLAG–CD9) was used. ILDR1–HA, ILDR2–HA and LSR–HA were specifically coprecipitated with FLAG–tricellulin. They were also coprecipitated with FLAG–occludin to lesser extents, but not with FLAG–marveled3-1 (Fig. 4). A trace amount of ILDR2–HA bound to FLAG–marveld3-2 was detected. These findings indicate that LSR, ILDR1 and ILDR2 can bind to tricellulin and occludin in living cells, and that their affinities for tricellulin are stronger than those for occludin, which may explain the selective concentration of tricellulin into TCs. We did not detect coprecipitation of endogenous tricellulin with LSR, ILDR1 or ILDR2 from lysates of EpH4 cells or epithelial tissues, possibly because of the solubilization problem of cell–cell junctions that are tightly associated with plaque proteins and cytoskeletons.

Characterization of ILDR1 and ILDR2 in epithelial barrier function

LSR-kd cells exhibited decreased TER (supplementary material Fig. S5A), as reported previously (Masuda et al., 2011), indicating that LSR contributes to epithelial barrier function. Thus, we examined whether ILDR1 and ILDR2 also support epithelial barrier function by comparing the TER and paracellular flux among parental EpH4 cells, LSR-kd cells, three independent clones of ILDR1–FLAG-expressing or ILDR2–FLAG-expressing LSR-kd cells and a mock-transfected clone of LSR-kd cells as the negative control. ILDR1–FLAG expression in LSR-kd cells restored the TER values (Fig. 5A), although these TER values were significantly lower than that for parental EpH4 cells ($P=0.00285$ for clone 1, $P=0.00010$ for clone 2 and $P=0.00011$ for clone 3). The ratio of the permeability of sodium (P_{Na}) and chloride (P_{Cl}) ions remained within a similar range in EpH4, LSR-kd, mock-transfected and ILDR1–FLAG-expressing LSR-kd cells (Fig. 5B,C). LSR-kd cells exhibited an increased flux of fluorescein (332 Da) and FITC–dextran at 4, 10 and 40 kDa as membrane-impermeable paracellular tracers, whereas ILDR1 expression restored the barrier (Fig. 5D–G) to all of these tracers, as observed in LSR–FLAG-expressing LSR-kd cells

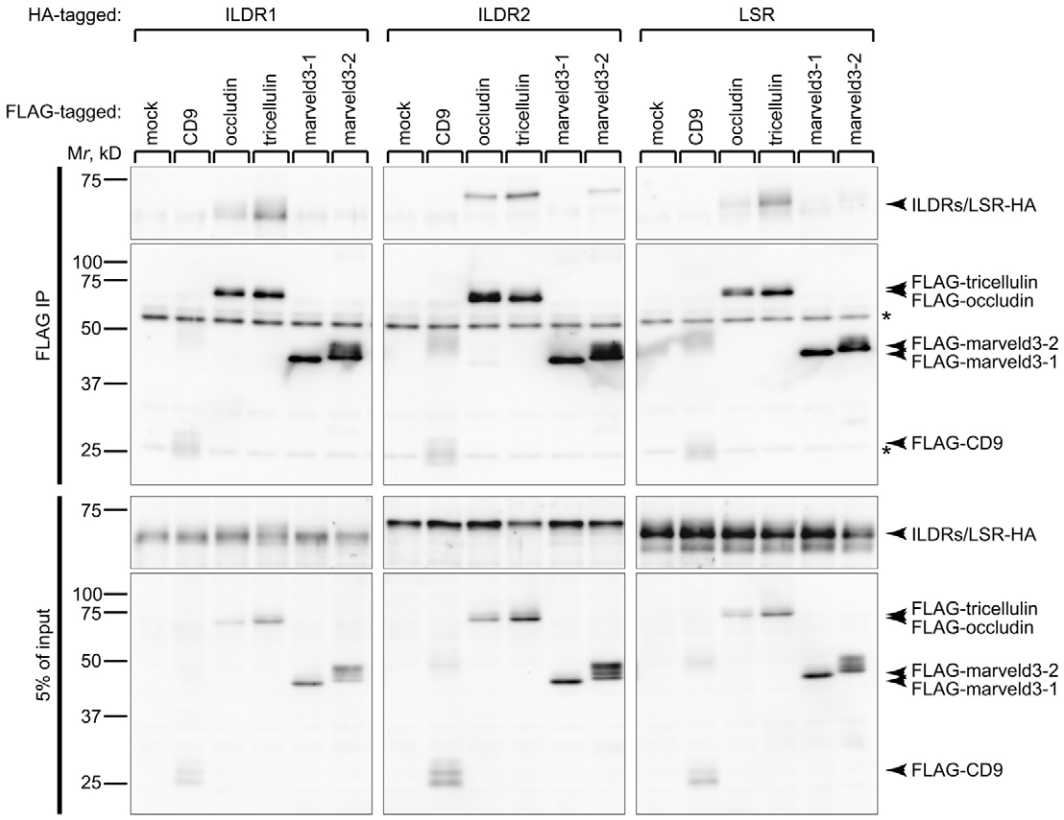

Fig. 4. Interaction between ILDR1, ILDR2 or LSR and tricellulin in living cells. HEK293T cells were transiently transfected with FLAG–CD9, FLAG–occludin, FLAG–tricellulin, FLAG–marveld3 variant 1 or FLAG–marveld3 variant 2 together with ILDR1–HA, ILDR2–HA or LSR–HA. FLAG-tagged proteins were immunoprecipitated (IP) from the cell lysates and subjected to immunoblotting using anti-HA and anti-FLAG mAbs. The asterisks indicate the heavy and light chains of the antibody used for the immunoprecipitation.

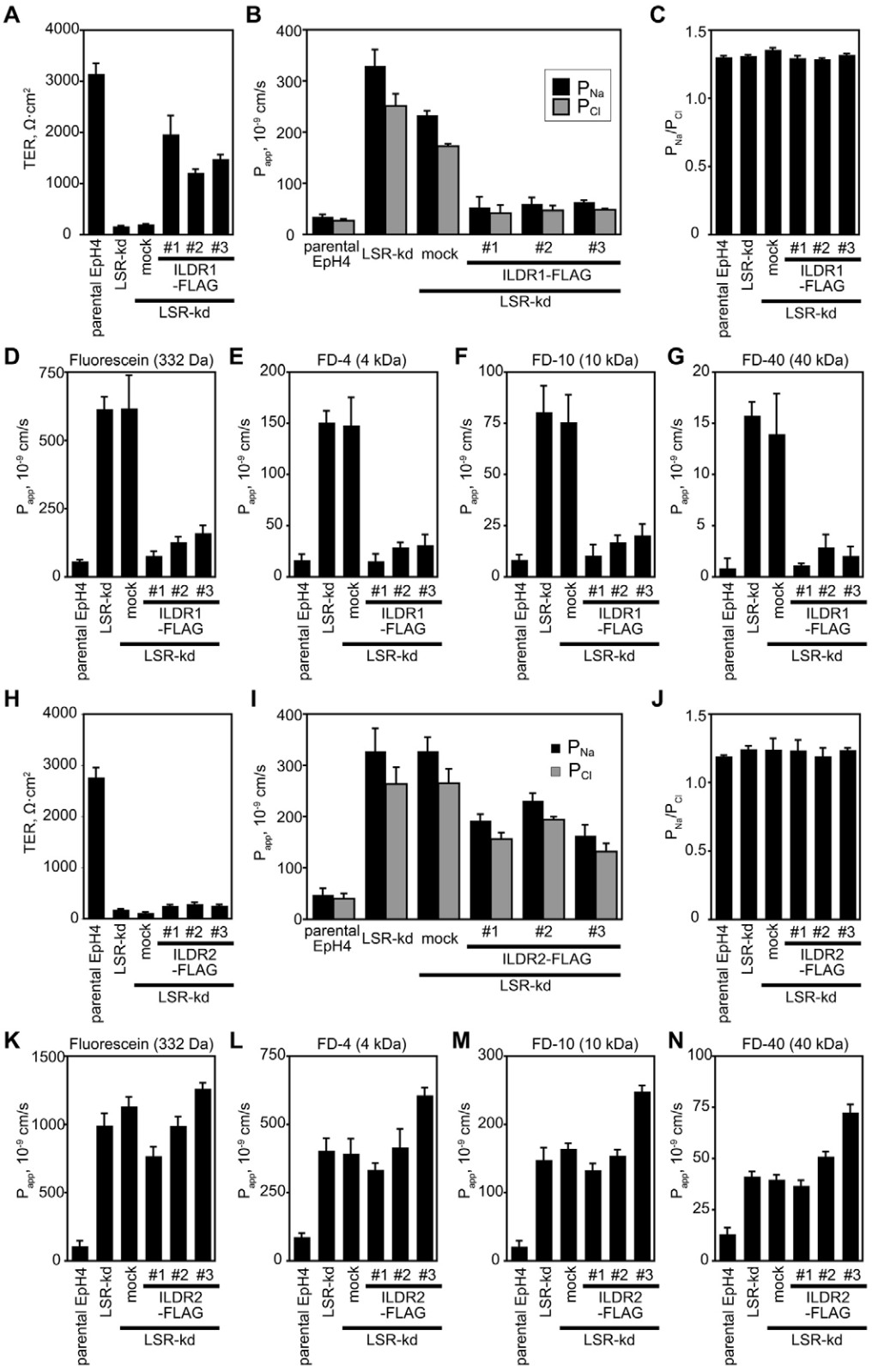

Fig. 5. Barrier functions of ILDR1- and ILDR2-expressing cells. (**A–G**) Barrier functions of cellular sheets of the three ILDR1-FLAG-expressing EpH4 clones. (**H–N**) Barrier function of cellular sheets of the three ILDR2–FLAG-expressing EpH4 clones. The barrier functions of the cellular sheets were evaluated by measuring the TER (A,H), dilution potential for Na^+ and Cl^- (B,I) and permeability of paracellular flux markers comprising fluorescein (332 Da) (D,K), 4-kDa FITC–dextran (FD-4) (E,L), 10-kDa FITC–dextran (FD-10) (F,M) and 40-kDa FITC–dextran (FD-40) (G,N). The P_{Na}/P_{Cl} ratios were calculated from the data in B and I (C,J). In all measurements, parental EpH4 cells, LSR-kd and mock-expressing LSR-kd (mock) EpH4 cell clones were used as controls. All data are expressed as means ± s.d. (n=4).

(supplementary material Fig. S5D–G). On the other hand, the TER value of ILDR2-expressing LSR-kd cells was significantly higher than that of LSR-kd cells (Fig. 5H), but much lower than that of the parental EpH4 cells (P=0.00010 for clone 1, P=0.00010 for clone 2 and P=0.00010 for clone 3). Furthermore, ILDR2 expression did not restore the tracer flux of FITC–dextran at 4, 10 and 40 kDa in LSR-kd cells (Fig. 5K–N). These findings indicate that ILDR1 is involved in epithelial

barrier function, similar to LSR, whereas the contribution of ILDR2 to the epithelial barrier function is much lower than that of ILDR1 or LSR.

Behavior of DFNB42-associated human ILDR1 mutants

Recently, it has been reported that autosomal recessive mutations in the *ILDR1* gene cause the familial nonsyndromic deafness DFNB42 (Borck et al., 2011). Given the characteristics of ILDR1 clarified in the present study, it is reasonable to speculate that these mutations impair the roles of ILDR1 in the recruitment of tricellulin to TCs and maintenance of epithelial barrier function. To better understand the mechanism of this disease, we examined the expression of ILDR1 in the inner ear and the behavior of human ILDR1 (hILDR1) mutant proteins associated with DFNB42 in terms of their subcellular localizations and abilities to recruit tricellulin. As shown in Fig. 6, immunofluorescence staining of the inner ear in mice revealed that ILDR1 was expressed in the organ of Corti, stria vascularis, utricle and saccule and localized at the TCs of these epithelial cells. In contrast, LSR was only expressed at the TCs in the Claudius cells of the organ of Corti and the stria vascularis (supplementary material Fig. S6A). Expression of ILDR2 was not detected in the inner ear by immunofluorescence staining (supplementary material Fig. S6B). These findings indicate that ILDR1 is the major form among LSR, ILDR1 and ILDR2 in the inner ear epithelium.

Next, we investigated the involvement of DFNB42-associated hILDR1 mutant proteins in the localization at TCs and the recruitment of tricellulin using molecular cell biology techniques in cultured epithelial cells, because we could not examine these issues in the affected individuals. To date, ten mutations have been reported to cause DFNB42 (Borck et al., 2011). Among these, one mutation (c.3G>A) alters the initiation codon of hILDR1 and three mutations (c.59-5_88del, c.411delG and c.499+1G>A) cause truncation at the extracellular region of hILDR1. Since these four mutations are considered to abolish the expression of a functional hILDR1 protein, we investigated the other six mutations, which cause the amino acid changes: R97Q, Q195X, T345PfsX20, E379X, E394SfsX15 and R453Q (Fig. 7A). To assess the interactions of these mutant ILDR1 proteins with tricellulin, we overexpressed FLAG-tagged hILDR1 mutant proteins together with HA-tagged human tricellulin in HEK293T cells and conducted immunoprecipitation assays with an anti-FLAG antibody. As shown in Fig. 7B, R89Q, T345PfsX20, E379X, E394SfsX15 and R453Q bound to tricellulin at comparable amounts to wild-type hILDR1, whereas Q195X did not. Next, we transfected LSR-kd cells with the expression vectors for wild-type hILDR1 and the six mutant proteins (Fig. 7C). Immunofluorescence microscopy revealed that wild-type hILDR1 and R453Q were clearly localized to TCs and recruited tricellulin to TCs (Fig. 7D). T345PfsX20, E379X and E394SfsX15 exhibited diffuse localizations at the lateral membrane with occasional concentration at TCs, where tricellulin was recruited (Fig. 7D). R89Q and Q195X neither localized to TCs nor recruited tricellulin (Fig. 7D). The failure of R89Q to localize at TCs is unlikely to be caused simply by its low expression level, since R453Q, which showed the lowest expression, was clearly located at TCs (Fig. 7C,D). These findings indicate that the *ILDR1* gene mutations in DFNB42 affect the behavior of their protein products in the localization at TCs and recruitment of tricellulin.

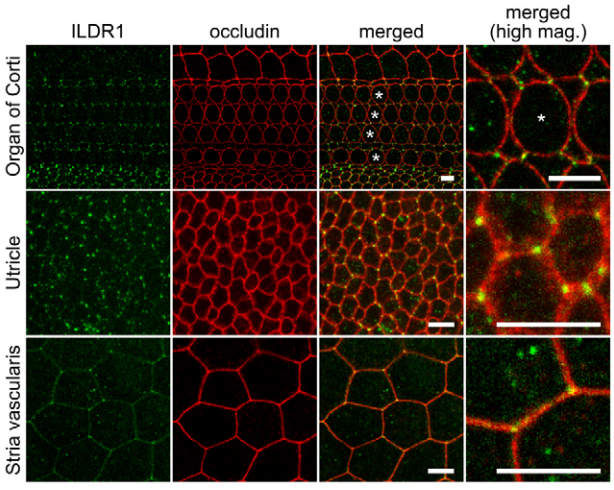

Fig. 6. Expression and localization of ILDR1 in the inner ear. Double immunofluorescence microscopy of the organ of Corti, utricle and stria vascularis in the inner ear using anti-ILDR1 pAb (green) and anti-occludin mAb (red). Optical sections of the organ of Corti and utricle obtained with a confocal microscope were stacked. The asterisks indicate hair cells. Scale bars: 50 μm. mag., magnification.

Impairment of TC localization of tricellulin mutants is associated with DFNB49

Mutations within the TRIC gene (also called *MARVELD2*), which encodes tricellulin, have been reported to cause another familial nonsyndromic deafness, DFNB49 (Riazuddin et al., 2006). All of the mutations identified not only in exons but also in splicing sites are predicted to finally cause truncation within the C-terminal cytoplasmic region of tricellulin (Fig. 8A), which has been shown to interact with LSR (Masuda et al., 2011). Thus, we speculated that the *TRIC* mutations in DFNB49 may hinder the interaction of the encoded tricellulin mutants with ILDR1 and disturb their localization at TCs in the inner ear epithelium. To examine this possibility, we evaluated whether these tricellulin mutants are recruited to TCs by ILDR1 in cultured epithelial cells. For this purpose, we established a stable tricellulin/LSR-double-knockdown EpH4 cell clone expressing hILDR1 (dKDhI1 cells) using an miRNA-based RNAi technique (supplementary material Fig. S7). Using dKDhI1 cells, we then obtained stable cell clones expressing wild-type human tricellulin or four human tricellulin mutant proteins with amino acid changes of C395fsX396, K445fsX449, K445fsX461 and R500X (Fig. 8A), which were encoded by the *TRIC* genes of DFNB49 patients reported previously (Riazuddin et al., 2006). As shown in Fig. 8B, all of the mutants were located to the cytoplasmic vesicles or plasma membrane without any concentration into TCs in dKDhI1 cells, whereas wild-type human tricellulin was clearly localized at TCs. These findings indicate that the DFNB49-associated mutations in *TRIC* disrupt the localizations of the tricellulin mutant proteins at TCs.

Discussion

tTJs are specialized structures of TJs at TCs, where the corners of three epithelial cells meet. To date, two integral membrane proteins, LSR and tricellulin, are known to be molecular components of tTJs, and both are required for the full barrier

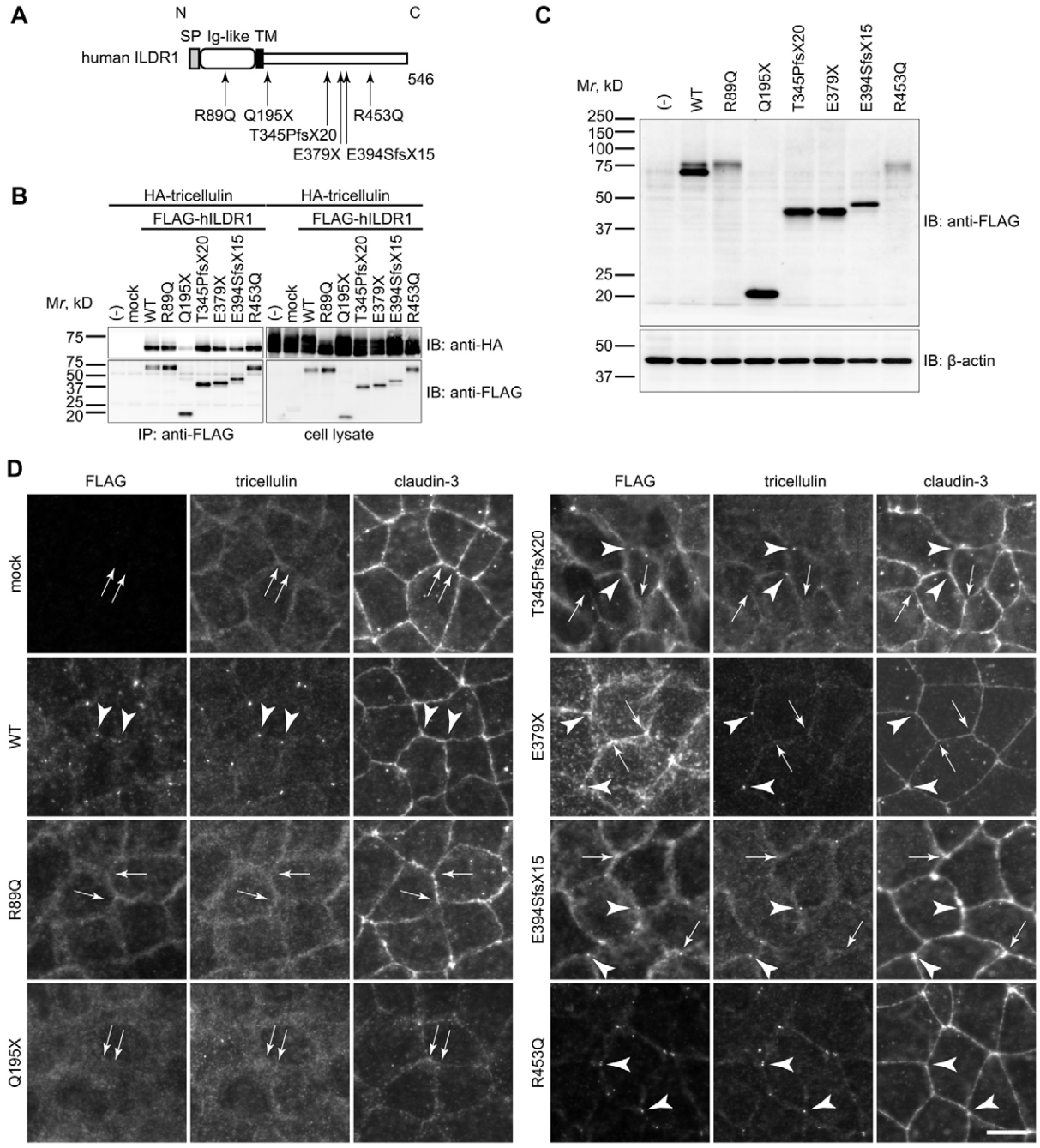

Fig. 7. Effects of DFNB42-associated mutations on the localization and tricellulin-recruiting function of ILDR1. (**A**) Schematic representation of the domain structure of human ILDR1 protein. The sites of the causative mutations of DFNB42 examined in the present study are indicated. (**B**) HEK293T cells were transiently transfected with FLAG–hILDR1 wild-type (WT), R89Q, Q195X, T345PfsX20, E379X, E394SfsX15 or R453Q together with human tricellulin–HA. The FLAG-tagged proteins were immunoprecipitated (IP) from cell lysates and subjected to immunoblotting (IB) using anti-HA and anti-FLAG mAbs. (**C**,**D**) LSR-kd cells stably expressing mock FLAG vector or FLAG-tagged human ILDR1 wild-type, R89Q, Q195X, T345PfsX20, E379X, E394SfsX15 or R453Q were subjected to immunoblotting with anti-FLAG and anti-β-actin mAbs (C) or immunostained with anti-FLAG mAb, anti-tricellulin mAb and anti-claudin-3 pAb (D). The arrowheads and arrows in D indicate TCs with and without tricellulin localization, respectively. Scale bar: 10 μm.

function of epithelial cellular sheets. Notably, LSR recruits tricellulin to tTJs. In the present study, we have shown that two LSR-related proteins, ILDR1 and ILDR2, share the common properties of localization at TCs and tricellulin recruitment with LSR. By analogy with LSR, it is reasonable to speculate that ILDR1 and ILDR2 are located to the central sealing element of tTJs at TCs. We also showed that tricellulin, among the TAMP family proteins, had the highest affinities for LSR, ILDR1 and ILDR2 in coprecipitation assays. These findings are consistent with the preferential tTJ localization of tricellulin among the TAMP members. In addition, we analyzed the pathogenesis of two types of familial deafness, DFNB42 and DFNB49, in terms

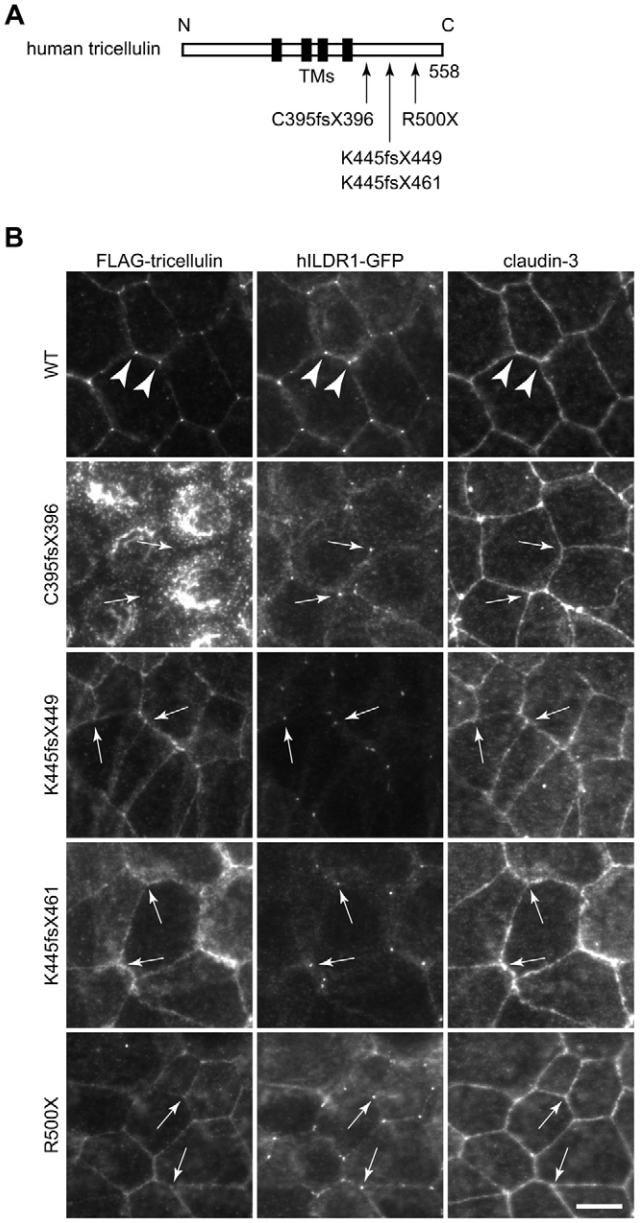

Fig. 8. Effects of DFNB49-associated mutations of tricellulin on its localization. (**A**) Schematic representation of the domain structure of human tricellulin protein. The sites of the causative mutations of DFNB49 examined in the present study are indicated. TMs, transmembrane domains. (**B**) Tricellulin/LSR-double-knockdown EpH4 cells expressing hILDR1 (dKDhI1 cells) stably transfected with wild-type (WT) or mutant human tricellulin were immunostained with anti-FLAG mAb, anti-tricellulin mAb and anti-claudin-3 pAb. The arrowheads and arrows indicate TCs with and without tricellulin localization, respectively. Scale bar: 10 μm.

of the impairment of the ILDR1–tricellulin system, in which ILDR1 recruits tricellulin to tTJs, in the inner ear epithelium. Based on the characteristic localizations of LSR, ILDR1 and ILDR2 at TCs, i.e. epithelial cell corners, and their evolutionary conservation, we propose to designate the protein family composed of these three proteins the 'angulin' family, which consists of angulin-1/LSR, angulin-2/ILDR1 and angulin-3/ILDR2, from the Latin word 'angulus' (meaning 'corner').

We investigated the contributions of the angulin family members to epithelial barrier function by expressing each of them in LSR-kd cells, followed by measurements of the TER and tracer flux. The LSR-kd cells exhibited decreased TER values and increased flux of tracer molecules compared with the parental EpH4 cells, as reported previously (Masuda et al., 2011), and re-expression of LSR restored the TER values and tracer flux to the levels in the parental EpH4 cells. When ILDR1 was expressed in LSR-kd cells, the TER values and tracer flux were also recovered, but not completely. In our experiment, the expression level of ILDR1–FLAG in LSR-kd cells appeared to be comparable to that of endogenous LSR in parental EpH4 cells (Fig. 3A). However, it was difficult to compare the extents of the TC concentrations of ILDR1–FLAG and LSR between these cells. At present, we are unable to conclude that ILDR1 has a completely redundant function with LSR to achieve the full barrier function of epithelial cellular sheets. On the other hand, the expression of a sufficiently high level of ILDR2 in LSR-kd cells increased the TER only slightly and did not restore the barrier function to enable tracer flux, despite tricellulin recruitment to TCs (Fig. 3A,B). These findings suggest that ILDR2 has a different function from LSR and ILDR1 and that recruitment of tricellulin to tTJs alone may not be sufficient for tight barriers at tTJs. ILDR2 is expressed in the epithelium surrounding neural tissues, including the perineurium, retinal pigment epithelium and choroid plexus. The distinct function of ILDR2 may contribute to the barrier property of such a specialized epithelium. Further investigations to compare the functions of LSR, ILDR1 and ILDR2 by expression of their deletion constructs or chimeric constructs in LSR-kd EpH4 cells will lead to a better understanding of this issue.

It has been proposed that the paracellular pathway is divided into two distinct routes (Van Itallie et al., 2008; Watson et al., 2001), namely the pore pathway and the leak pathway (Anderson and Van Itallie, 2009; Shen et al., 2011; Turner, 2009). The pore pathway has ion selectivity and a limited pore size of ~4 Å, and the leak pathway contributes to the passage of macromolecules. Krug et al. (Krug et al., 2009) showed that tTJ-restricted exogenous expression of a small amount of tricellulin increased the barrier to macromolecules but not to ions, whereas expression of a large amount of tricellulin in both bTJs and tTJs resulted in an increase of the barrier to both macromolecules and ions, using MDCK II cells, suggesting that tTJs are the pathways for macromolecules. From these results, they proposed that tTJs correspond to the leak (or large pore) pathway, whereas bTJs correspond to the pore (or small pore) pathway. In view of their model, our finding that LSR-kd cells exhibited increased permeability of ions in addition to tracer molecules across the cellular sheet may be interpreted as opening of both the pore pathway in bTJs and the leak pathway in tTJs. Therefore, the angulin family members might maintain the tightness of not only tTJ, but also bTJ pathways.

Mutations in the *TRIC* and *ILDR1* genes have been reported to cause the human familial nonsyndromic deafnesses DFNB49 and DFNB42, respectively. In relation to this, it has been reported that ablations or mutations of the genes for TJ proteins expressed in the organ of Corti cause deafness. For example, mutations in the *CLDN14* gene, which encodes claudin-14, cause the familial nonsyndromic deafness DFNB29 (MIM 614035) (Wilcox et al., 2001), and claudin-14-knockout mice also exhibit hearing loss (Ben-Yosef et al., 2003). Furthermore, a mutation in the *Cldn9*

gene, which encodes claudin-9, causes deafness in mice (Nakano et al., 2009). Both claudin-14 and claudin-9 are components of TJs in the reticular lamina in the organ of Corti (Ben-Yosef et al., 2003; Nakano et al., 2009; Nunes et al., 2006). Physiological analyses of the claudin-14-deficient mice and claudin-9 mutant mice suggested that loss of the barrier function of TJs at the reticular lamina increases the flux of K^+ from the apical endolymph to the basolateral extracellular space, leading to death of the outer hair cells by prolonged exposure to high concentrations of K^+. Given our observations that the angulin family proteins, including ILDR1, recruit tricellulin to TCs and contribute to epithelial barrier function, we hypothesized that loss of the TC localization of ILDR1 or tricellulin mutants causes impairment of epithelial barrier function in the organ of Corti. Consistently, we found that, among the angulin family proteins, ILDR1 was dominantly expressed in the organ of Corti, particularly in the region around hair cells in mice, suggesting that ILDR1 is required for the tricellulin recruitment and epithelial barrier function in this region.

To further examine the mechanisms underlying deafness, we analyzed the localizations of human ILDR1 and tricellulin mutant proteins associated with DFNB42 and DFNB49 in cultured epithelial cells. Our analysis of the hILDR1 mutants revealed that two mutations (R97Q and Q195X) abolished the localization to TCs and tricellulin-recruiting function, and that three other mutants (T345PfsX20, E379X and E394SfsX15) exhibited reduced localization of tricellulin at TCs, supporting our hypothesis. Regarding the latter three mutants, another possibility should also be considered to explain the pathogenesis. It is well known that mRNAs with premature truncation upstream of exon–exon junctions undergo degradation by the mechanism designated nonsense-mediated mRNA decay (NMD) (Frischmeyer and Dietz, 1999). Since T345PfsX20, E379X and E394SfsX15 cause truncation within exons other than the last exon, the mRNAs of these mutants may be degraded by the NMD mechanism *in vivo*, whereas the cDNAs of these mutants were expressed without degradation in our experiments. If the expression levels of these ILDR1 mutant proteins are insufficient in the patients, tricellulin would be mislocalized. On the contrary, R453Q was capable of localizing at TCs and recruiting tricellulin, although it did not seem to undergo NMD. Since the linkage of the R453Q mutation to DFNB42 is relatively low (logarithm of odds score=2.1) and the Arg453 residue is not completely conserved among the orthologs and paralogs of ILDR1, Borck et al. (Borck et al., 2011) suspended a conclusion about the pathogenicity of the R453Q mutation. Further studies on this mutation will reveal its detailed pathogenicity. In the case of the tricellulin mutations associated with DFNB49, none of the mutated tricellulin proteins that we analyzed were recruited to TCs by ILDR1 in cultured epithelial cells, supporting our hypothesis. To date, the tricellulin gene mutations associated with DFNB49 have been located within the region encoding the C-terminal cytoplasmic domain of tricellulin. This seems reasonable, since a recombinant CD9 protein fused with the C-terminal cytoplasmic domain of tricellulin was recruited by LSR (Masuda et al., 2011), suggesting that this domain is required for the TC localization of tricellulin by angulin family proteins.

In summary, we found that the angulin family proteins LSR, ILDR1 and ILDR2 (we propose to designate them angulin-1, angulin-2 and angulin-3, respectively) share the common characteristics of localization at TCs and tricellulin recruitment, and that tTJs are heterogeneous in terms of their molecular contents. At present, it is not yet fully understood how tTJs are established and to what extent tTJs contribute to homeostasis of the vertebrate body. Further analyses of LSR, ILDR1 and ILDR2 should lead to better understanding of the molecular mechanism and cell type-dependent significance of tTJs.

Materials and Methods

cDNA cloning, sequencing and plasmid construction

cDNAs encoding mouse LSR (aa 1–575) and mouse tricellulin-a (aa 1–555) were described previously (Ikenouchi et al., 2005; Masuda et al., 2011). Total RNA was isolated from mouse tissues and the mouse mammary epithelial cell line EpH4 according to a previously developed method (Chomczynski and Sacchi, 1987). Antibody production and the isolation of mouse tissues were approved by the Institutional Animal Care and Use Committee, and carried out according to the Kobe University Animal Experimentation Regulations. cDNA libraries were synthesized using a cDNA synthesis kit (TaKaRa Bio Inc.) or SuperScript III reverse transcriptase (Invitrogen). cDNAs encoding mouse ILDR1 (aa 1–537; NCBI accession number AK136284), mouse ILDR2 (aa 1–627; NCBI accession number FJ024498), mouse marveld3 variant 1 (aa 1–376; NCBI accession number NM_028584), mouse marveld3 variant 2 (aa 1–385; NCBI accession number NM_212447) and mouse CD9 (aa 1–226) were amplified by PCR with KOD -Plus- DNA polymerase (Toyobo) using the lung, eye, small intestine, (for marveld3 variants 1 and 2) and lung cDNA libraries as templates, respectively. cDNAs encoding human ILDR1 (aa 1–546; NCBI accession number AY672837) and human tricellulin-a (aa 1–558) were amplified by PCR using KOD -Plus- DNA polymerase and a human lung Marathon cDNA library (Clontech) as a template. All of the *Bam*HI and *Eco*RI sites within the DNA fragments were disrupted by introducing silent mutations. The DNA fragments were then subcloned into the pBluescript II SK+ vector (Stratagene) with *Bam*HI and *Eco*RI sites, and the DNA sequences were confirmed. For expression in mammalian cells, the DNA fragments were subcloned into pCAG vectors with N-terminal 3×HA (YPYDVPDYA) tags, C-terminal 3×HA tags, N-terminal 1×FLAG (DYKDDDDK) tag and 2×Strep II (WSHPQFEK) tags or C-terminal 2×FLAG tags. All of these vectors were generated by insertion of a multiple cloning site and tag sequences into the *Eco*RI site of pCAGGSneodel*Eco*RI (Niwa et al., 1991). For the generation of LSR/tricellulin-double-knockdown and human ILDR1–EGFP-expressing cells, human ILDR1 was conjugated with EGFP and miRNA-based shRNAs against LSR and tricellulin, and subcloned into pCAG vector (see details in supplementary material Fig. S7). For bacterial expression, DNA fragments were amplified with KOD -Plus- DNA polymerase and subcloned into the pGEX-2T vector (GE Healthcare) for GST-fused proteins or the pMal-c2x vector (New England Biolabs) for MBP-fused proteins, and the DNA sequences were confirmed.

Antibodies and cells

The rat anti-occludin mAb (MOC37), rabbit anti-occludin pAb (Saitou et al., 1997), mouse anti-ZO-1 mAb (T8-754) (Itoh et al., 1991), rabbit anti-LSR pAb (Masuda et al., 2011) and rat anti-tricellulin mAb (24–69) (Ikenouchi et al., 2005) were as described previously. The rat anti-HA mAb (3F10), rabbit anti-claudin-3 pAb, mouse anti-β-actin mAb (AC-15), rat anti-GFP mAb (RQ2) and mouse anti-GFP mAb (7.1 and 13.1) were purchased from Roche, Invitrogen, Sigma, MBL and Roche, respectively. The mouse anti-HA (4B2) and mouse anti-DYKDDDDK (FLAG) (1E6) mAbs were purchased from Wako Chemicals. For the generation of rabbit anti-mouse ILDR1 and rabbit anti-mouse ILDR2 pAbs, GST–mouse ILDR1 (aa 259–537) and GST–mouse ILDR2 (aa 384–627) were produced using *Escherichia coli* strain BL21 and purified using glutathione–Sepharose (GE Healthcare) according to the manufacturer's instructions. The purified proteins were dialyzed against phosphate-buffered saline (PBS) and used for immunization of rabbits by Keari Co. Ltd. For affinity-purification of antisera, MBP–ILDR1 (aa 259–537) and MBP–ILDR2 (aa 384–627) were produced using *E. coli* strain BL21, purified using amylose resin (New England Biolabs) and applied for purification of the anti-ILDR1 and anti-ILDR2 antisera using MBP-fusion proteins and CNBr-activated Sepharose (GE Healthcare) according to the manufacturer's instructions. Rat anti-mouse LSR mAb was raised against GST–mouse LSR (aa 361–531) by the immunization of Wistar rats as described previously (Saitou et al., 1997).

Cy3-conjugated goat anti-rabbit IgG and Cy3-conjugated donkey anti-mouse IgG were purchased from Jackson ImmunoResearch Laboratories. Alexa 488-conjugated donkey anti-rat IgG and Alexa 647-conjugated donkey anti-rabbit IgG were obtained from Invitrogen Molecular Probes. Horseradish peroxidase (HRP)-linked donkey anti-rabbit IgG and HRP-linked goat anti-rat IgG were purchased from GE Healthcare. HRP-linked goat anti-mouse IgG was from Promega.

Mouse mammary epithelial cells (EpH4), mouse fibroblast cells (NIH/3T3) and human embryonic kidney cells (HEK293T) were cultured in Dulbecco's modified Eagle's medium (DMEM) supplemented with 10% fetal calf serum.

Transfection and establishment of stable cell clones

On the day before transfection, cells were seeded on 24-well or 12-well plates. After replacement of the medium with DMEM containing 50 μM $CaCl_2$, the cells were transfected using Lipofectamine LTX with Plus Reagent (Invitrogen) according to the forward transfection methods provided by the manufacturer. For the establishment of stable cell clones, the cells were replated on to 96-well plates and selected by addition of 400 μg/ml G-418 (Nacalai Tesque) or 2 μg/ml Puromycin (Sigma-Aldrich).

Immunoblotting

For immunoblotting of cell lysates, cells were scraped in Laemmli SDS sample buffer and boiled for 5 minutes. The proteins were separated by one-dimensional SDS-PAGE and electrotransferred from the gels on to nitrocellulose membranes, followed by incubation with the primary antibodies. The bound antibodies were detected using HRP-linked secondary antibodies and enhanced chemiluminescence (ECL Prime Kit; GE Healthcare).

Immunofluorescence microscopy

For immunofluorescence microscopy of cultured cells, cells cultured on coverslips were fixed with 1% formaldehyde in PBS containing 1 mM $CaCl_2$ for 10 minutes at room temperature, permeabilized with 0.2% (w/v) Triton X-100 in PBS for 10 minutes and washed with PBS three times. For immunofluorescence microscopy of frozen sections of mouse tissues, dissected tissue blocks were embedded in OCT compound (Sakura Finetek Japan), quickly frozen in liquid nitrogen and cut into ~6-μm-thick sections in a cryostat at −20℃. The sections were mounted on coverslips, air-dried for 30 minutes and fixed with 95% ethanol at −20℃ for 20 minutes followed by 100% acetone treatment at room temperature for 1 minute. For immunofluorescence microscopy of mouse inner ear tissues, the inner ears of postnatal day 3 mice were dissected and fixed for 20 minutes by injection of 10% (w/v) trichloroacetic acid through the oval and round windows. After 20 minutes, the tissues were washed with PBS, microdissected into the organ of Corti, stria vascularis and vestibule, and permeabilized by incubation with PBS containing 0.2% (w/v) Triton X-100 for 30 minutes at room temperature. For immunofluorescence microscopy of the mouse olfactory epithelium, the tissue was dissected, fixed for 20 minutes in 10% (w/v) trichloroacetic acid, washed with PBS and permeabilized with PBS containing 0.2% (w/v) Triton X-100 for 30 minutes at room temperature.

All of the samples were blocked with 2% BSA in PBS and incubated with a primary antibody followed by a fluorescence-labeled secondary antibody. After washing with PBS, the samples were embedded in FluorSave reagent (Calbiochem) and observed with a fluorescence microscope (IX71; Olympus). Photographs were recorded with a cooled charge-coupled device camera (ORCA-ER; Hamamatsu Photonics K.K.) controlled by a Power Macintosh G5 and the software package IPLab V3.9.5 (BD Biosciences). For observation of the inner ear tissues and olfactory epithelium, a confocal microscope (TCS SPE; Leica Microsystems) was used. Samples were observed at room temperature.

Immunoelectron microscopy

The mouse olfactory epithelium was dissected and fixed with 50 mM HEPES-NaOH (pH 7.4) containing 2% formaldehyde, 0.05% glutaraldehyde and 5% sucrose for 2 hours at room temperature. An antigen retrieval reaction was then performed using Immunosaver solution (Nisshin EM Ltd). Briefly, tissue blocks of ~1-mm thickness were soaked in 0.1% semicarbazide hydrochloric acid solution for 1 hour at room temperature, washed with 0.1 M phosphate buffer (PB) (pH 7.4) and distilled water, and soaked in Immunosaver solution at 70℃ for 16 hours. The blocks were permeabilized with PBS containing 0.2% (w/v) Triton X-100 for 20 minutes at room temperature and treated with the anti-ILDR1 pAb in PBS containing 0.4% BSA for 1 hour at room temperature followed by an anti-rabbit antibody conjugated with 1.4-nm Nanogold particles (Nanoprobes) in PBS containing 0.4% BSA for 16 hours at 4℃. After fixation with 1% glutaraldehyde in 0.1 M PB for 15 minutes at room temperature, the blocks were washed extensively with 0.1 M PB and rinsed with distilled water. Silver enhancement was performed using HQ Silver (Nanoprobes) and the samples were postfixed with 0.5% OsO_4 in 0.1 M PB for 15 minutes at 4℃, followed by dehydration in an ethanol series (65%, 75%, 85%, 95%, 99% and 100%) and propylene oxide and embedding in Epon 812 resin. Ultrathin sections of ~70-nm thickness were stained with 1% hafnium chloride in methanol and lead citrate, and then observed under an electron microscope (JEM-1011; JEOL).

Immunoprecipitation

HEK293T cells were transfected with expression vectors using Lipofectamine LTX with Plus Reagent. At 2 days after transfection, the cells were washed once with PBS, scraped in ice-cold lysis buffer [50 mM Tris-HCl (pH 7.4), 150 mM NaCl, 2 mM EDTA, 1 mM DTT, 0.5% Nonidet P-40 and 1 mM DTT] and incubated at 4℃ for 20 minutes. The cell lysates were centrifuged at 4℃ for 20 minutes at 15,000×***g*** and the supernatants were precleared with Protein G–Sepharose beads by incubation at 4℃ for 30 minutes. After removal of the beads by centrifugation, the appropriate antibody was added and incubated at 4℃ for 2 hours. Protein G–Sepharose beads were then added and incubated at 4℃ for 30 minutes. After washing, the bound proteins were eluted with SDS sample buffer and analyzed by SDS-PAGE followed by immunoblotting.

Semi-quantitative analysis of mRNA in cells and tissues

cDNA libraries isolated from EpH4 cells and tissues were amplified with primers for mouse LSR (5′-CGCAGAGCTCATTGTCCTTGATTG-3′ and 5′-GGAGGTTACT-TCACTCATGGCCCG; target, 541 bp), mouse ILDR1 (5′-TGAACCCGCTGCT-GCAGCGAGAT-3′ and 5′-CTATGGGAGCTCTCTCTCTCCAAG-3′; target, 834 bp), mouse ILDR2 (5′-TCAGTGGAACTGCTGGTGTTGGAG-3′ and 5′-GATTTGGAGCGCTGCTGGCTGTGC-3′; target, 692 bp) and mouse GAPDH (5′-CCAGAACATCATCCCTGCATC-3′ and 5′-CCTGCTTCACCACCTTCTT-GA-3′; target, 185 bp) using Ex Taq DNA polymerase (TaKaRa Bio Inc.) or KOD -Plus- DNA polymerase. pBluescript II SK+ vectors containing mouse LSR, mouse ILDR1 and mouse ILDR2 at known concentrations were used as standards. The amplified products were resolved on ethidium bromide-stained 1.25% agarose gels and photographed under a UV light source.

TER and paracellular tracer flux

Electrophysiological studies were performed as described previously (Tokuda et al., 2009; Tokuda et al., 2010) with minor modifications. EpH4 cells were subcultured daily for the preceding 2 days to obtain a nonaggregated cell suspension. The cells were seeded on polycarbonate Transwell filters (Corning) with a 12-mm diameter and 0.4-μm pore size at a density of 1.0×10^5 cells/cm^2, and the culture medium was changed every day from 2 days after cell seeding. Four filters were used for each cell line. The TER of confluent monolayers of cells was determined in culture medium as described previously (Masuda et al., 2011) using a Millicell-ERS epithelial volt-ohm meter (Millipore) with subtraction of the resistance of a blank filter. To determine the ion permeabilities of Na^+ (P_{Na}) and Cl^- (P_{Cl}), the dilution potentials and TER values of monolayers of cells grown on filters for 6 days were measured at 37℃ with solution A [140 mM NaCl, 5 mM glucose, 5 mM KCl, 1 mM $MgCl_2$, 1 mM $CaCl_2$ and 10 mM HEPES-NaOH (pH 7.4)] on the apical side and solution B [70 mM NaCl, 130 mM sucrose, 5 mM glucose, 5 mM KCl, 1 mM $MgCl_2$, 1 mM $CaCl_2$ and 10 mM HEPES-NaOH (pH 7.4)] on the basolateral side. The electrical potentials and TER values obtained from a blank filter under the same conditions were subtracted. The stabilities of the transepithelial voltage and TER were confirmed by repeated measurements for at least 5 minutes. The P_{Na}/P_{Cl} ratio was calculated using the Goldman–Hodgkin–Katz equation. The values for P_{Na} and P_{Cl} were then calculated from the TER and P_{Na}/P_{Cl} using the Kimizuka–Koketsu equation (Kimizuka and Koketsu, 1964). For measurements of tracer flux, fluorescein or FITC–dextran dissolved in DMEM without Phenol Red was added to the upper well at a concentration of 1 mg/ml at day 6. After 2 hours, an aliquot of the medium in the lower well was collected and the fluorescence at 518 nm was measured using a fluorescence spectrophotometer (F-4500; Hitachi High-Tech) with an excitation wavelength of 488 nm. The amount of fluorescein or FITC–dextran was determined by extrapolation from a standard curve of known fluorescein or FITC–dextran concentrations using linear regression. The apparent permeability was calculated using the equation $P_{app}=(dQ/dt)/AC_0$, where dQ/dt is the rate at which the compound appears in the receiver well, A is the surface area of the filter and C_0 is the initial concentration of the donor well (Van Itallie et al., 2008; Watson et al., 2001).

Bioinformatics analysis

To obtain LSR-related protein sequences, we first conducted a BLAST search (http://blast.ncbi.nlm.nih.gov/Blast.cgi) using the mouse LSR amino acid sequence (AK146807) with the setting of organism '*Mus musculus*' and obtained 25 sequences with significant homology to LSR (E-value <0.05). All of these sequences were complete or partial sequences of LSR, ILDR1 and ILDR2. Besides, according to the EMBL-EBI database (http://www.ebi.ac.uk/), three InterPro domains, immunoglobulin subtype (IPR003599), LISCH7 (IPR008664) and immunoglobulin-like fold (IPR013783), are annotated within the LSR sequence, and only LSR, ILDR1 and ILDR2 are annotated for all of these three domains. Thus, we concluded that ILDR1 and ILDR2 are the only paralogs of LSR within the mouse genome. Next, we tried to examine the evolutionary conservation of the angulin family proteins. The amino acid sequences of human, mouse, chick, African clawed frog, Western clawed frog and zebrafish LSR, ILDR1 and ILDR2 were aligned and a phylogenetic tree was drawn by the neighbor-joining method using the ClustalX (http://www.clustal.org/) and NJplot (http://pbil.univ-lyon1.fr/software/njplot.html) software packages (Larkin et al., 2007; Perrière and Gouy, 1996; Saitou and Nei, 1987). The bootstrap values were calculated by the ClustalX package using the default settings.

Acknowledgements

We thank Kyoko Furuse for her technical assistance in the electron microscopy, and Keisuke Nagao, Masayuki Amagai, Shigenobu

Yonemura, Akira Nagafuchi and all the members of the Mikio Furuse laboratory for their helpful discussions.

Author contributions

T.H. and M.F. planned the experimental design and wrote the paper. T.H., S.T., S.K. and H.N. conducted the experiments and analyzed the data. S.M. and Y.O. contributed reagents.

Funding

This work was supported by a Funding Program for Next Generation World Leading Researchers (NEXT Program) from the Japan Society for the Promotion of Science initiated by the Council for Science and Technology Policy [grant number LS084 to M.F]. T.H. is a research fellow of the Japan Society for the Promotion of Science.

Supplementary material available online at
http://jcs.biologists.org/lookup/suppl/doi:10.1242/jcs.116442/-/DC1

References

Anderson, J. M. and Van Itallie, C. M. (2009). Physiology and function of the tight junction. *Cold Spring Harb. Perspect. Biol.* **1**, a002584.

Angelow, S., Ahlstrom, R. and Yu, A. S. (2008). Biology of claudins. *Am. J. Physiol. Renal Physiol.* **295**, F867-F876.

Ben-Yosef, T., Belyantseva, I. A., Saunders, T. L., Hughes, E. D., Kawamoto, K., Van Itallie, C. M., Beyer, L. A., Halsey, K., Gardner, D. J., Wilcox, E. R. et al. (2003). Claudin 14 knockout mice, a model for autosomal recessive deafness DFNB29, are deaf due to cochlear hair cell degeneration. *Hum. Mol. Genet.* **12**, 2049-2061.

Borck, G., Ur Rehman, A., Lee, K., Pogoda, H. M., Kakar, N., von Ameln, S., Grillet, N., Hildebrand, M. S., Ahmed, Z. M., Nürnberg, G. et al. (2011). Loss-of-function mutations of ILDR1 cause autosomal-recessive hearing impairment DFNB42. *Am. J. Hum. Genet.* **88**, 127-137.

Chishti, M. S., Bhatti, A., Tamim, S., Lee, K., McDonald, M. L., Leal, S. M. and Ahmad, W. (2008). Splice-site mutations in the TRIC gene underlie autosomal recessive nonsyndromic hearing impairment in Pakistani families. *J. Hum. Genet.* **53**, 101-105.

Chomczynski, P. and Sacchi, N. (1987). Single-step method of RNA isolation by acid guanidinium thiocyanate-phenol-chloroform extraction. *Anal. Biochem.* **162**, 156-159.

Dokmanovic-Chouinard, M., Chung, W. K., Chevre, J. C., Watson, E., Yonan, J., Wiegand, B., Bromberg, Y., Wakae, N., Wright, C. V., Overton, J. et al. (2008). Positional cloning of "Lisch-Like", a candidate modifier of susceptibility to type 2 diabetes in mice. *PLoS Genet.* **4**, e1000137.

Farquhar, M. G. and Palade, G. E. (1963). Junctional complexes in various epithelia. *J. Cell Biol.* **17**, 375-412.

Friend, D. S. and Gilula, N. B. (1972). Variations in tight and gap junctions in mammalian tissues. *J. Cell Biol.* **53**, 758-776.

Frischmeyer, P. A. and Dietz, H. C. (1999). Nonsense-mediated mRNA decay in health and disease. *Hum. Mol. Genet.* **8**, 1893-1900.

Furuse, M. and Tsukita, S. (2006). Claudins in occluding junctions of humans and flies. *Trends Cell Biol.* **16**, 181-188.

Hauge, H., Patzke, S., Delabie, J. and Aasheim, H. C. (2004). Characterization of a novel immunoglobulin-like domain containing receptor. *Biochem. Biophys. Res. Commun.* **323**, 970-978.

Ikenouchi, J., Furuse, M., Furuse, K., Sasaki, H., Tsukita, S. and Tsukita, S. (2005). Tricellulin constitutes a novel barrier at tricellular contacts of epithelial cells. *J. Cell Biol.* **171**, 939-945.

Itoh, M., Yonemura, S., Nagafuchi, A., Tsukita, S. and Tsukita, S. (1991). A 220-kD undercoat-constitutive protein: its specific localization at cadherin-based cell-cell adhesion sites. *J. Cell Biol.* **115**, 1449-1462.

Kimizuka, H. and Koketsu, K. (1964). Ion transport through cell membrane. *J. Theor. Biol.* **6**, 290-305.

Krug, S. M., Amasheh, S., Richter, J. F., Milatz, S., Günzel, D., Westphal, J. K., Huber, O., Schulzke, J. D. and Fromm, M. (2009). Tricellulin forms a barrier to macromolecules in tricellular tight junctions without affecting ion permeability. *Mol. Biol. Cell* **20**, 3713-3724.

Larkin, M. A., Blackshields, G., Brown, N. P., Chenna, R., McGettigan, P. A., McWilliam, H., Valentin, F., Wallace, I. M., Wilm, A., Lopez, R. et al. (2007). Clustal W and Clustal X version 2.0. *Bioinformatics* **23**, 2947-2948.

Masuda, S., Oda, Y., Sasaki, H., Ikenouchi, J., Higashi, T., Akashi, M., Nishi, E. and Furuse, M. (2011). LSR defines cell corners for tricellular tight junction formation in epithelial cells. *J. Cell Sci.* **124**, 548-555.

Nakano, Y., Kim, S. H., Kim, H. M., Sanneman, J. D., Zhang, Y., Smith, R. J., Marcus, D. C., Wangemann, P., Nessler, R. A. and Bánfi, B. (2009). A claudin-9-based ion permeability barrier is essential for hearing. *PLoS Genet.* **5**, e1000610.

Niwa, H., Yamamura, K. and Miyazaki, J. (1991). Efficient selection for high-expression transfectants with a novel eukaryotic vector. *Gene* **108**, 193-199.

Nunes, F. D., Lopez, L. N., Lin, H. W., Davies, C., Azevedo, R. B., Gow, A. and Kachar, B. (2006). Distinct subdomain organization and molecular composition of a tight junction with adherens junction features. *J. Cell Sci.* **119**, 4819-4827.

Perrière, G. and Gouy, M. (1996). WWW-query: an on-line retrieval system for biological sequence banks. *Biochimie* **78**, 364-369.

Raleigh, D. R., Marchiando, A. M., Zhang, Y., Shen, L., Sasaki, H., Wang, Y., Long, M. and Turner, J. R. (2010). Tight junction-associated MARVEL proteins marveld3, tricellulin, and occludin have distinct but overlapping functions. *Mol. Biol. Cell* **21**, 1200-1213.

Riazuddin, S., Ahmed, Z. M., Fanning, A. S., Lagziel, A., Kitajiri, S., Ramzan, K., Khan, S. N., Chattaraj, P., Friedman, P. L., Anderson, J. M. et al. (2006). Tricellulin is a tight-junction protein necessary for hearing. *Am. J. Hum. Genet.* **79**, 1040-1051.

Saitou, N. and Nei, M. (1987). The neighbor-joining method: a new method for reconstructing phylogenetic trees. *Mol. Biol. Evol.* **4**, 406-425.

Saitou, M., Ando-Akatsuka, Y., Itoh, M., Furuse, M., Inazawa, J., Fujimoto, K. and Tsukita, S. (1997). Mammalian occludin in epithelial cells: its expression and subcellular distribution. *Eur. J. Cell Biol.* **73**, 222-231.

Schneeberger, E. E. and Lynch, R. D. (2004). The tight junction: a multifunctional complex. *Am. J. Physiol. Cell Physiol.* **286**, C1213-C1228.

Shen, L., Weber, C. R., Raleigh, D. R., Yu, D. and Turner, J. R. (2011). Tight junction pore and leak pathways: a dynamic duo. *Annu. Rev. Physiol.* **73**, 283-309.

Songyang, Z., Fanning, A. S., Fu, C., Xu, J., Marfatia, S. M., Chishti, A. H., Crompton, A., Chan, A. C., Anderson, J. M. and Cantley, L. C. (1997). Recognition of unique carboxyl-terminal motifs by distinct PDZ domains. *Science* **275**, 73-77.

Staehelin, L. A. (1973). Further observations on the fine structure of freeze-cleaved tight junctions. *J. Cell Sci.* **13**, 763-786.

Staehelin, L. A., Mukherjee, T. M. and Williams, A. W. (1969). Freeze-etch appearance of the tight junctions in the epithelium of small and large intestine of mice. *Protoplasma* **67**, 165-184.

Steed, E., Rodrigues, N. T., Balda, M. S. and Matter, K. (2009). Identification of MarvelD3 as a tight junction-associated transmembrane protein of the occludin family. *BMC Cell Biol.* **10**, 95.

Tokuda, S., Miyazaki, H., Nakajima, K., Yamada, T. and Marunaka, Y. (2009). Hydrostatic pressure regulates tight junctions, actin cytoskeleton and transcellular ion transport. *Biochem. Biophys. Res. Commun.* **390**, 1315-1321.

Tokuda, S., Miyazaki, H., Nakajima, K., Yamada, T. and Marunaka, Y. (2010). NaCl flux between apical and basolateral side recruits claudin-1 to tight junction strands and regulates paracellular transport. *Biochem. Biophys. Res. Commun.* **393**, 390-396.

Turner, J. R. (2009). Intestinal mucosal barrier function in health and disease. *Nat. Rev. Immunol.* **9**, 799-809.

Van Itallie, C. M., Holmes, J., Bridges, A., Gookin, J. L., Coccaro, M. R., Proctor, W., Colegio, O. R. and Anderson, J. M. (2008). The density of small tight junction pores varies among cell types and is increased by expression of claudin-2. *J. Cell Sci.* **121**, 298-305.

Wade, J. B. and Karnovsky, M. J. (1974). The structure of the zonula occludens. A single fibril model based on freeze-fracture. *J. Cell Biol.* **60**, 168-180.

Walker, D. C., MacKenzie, A., Hulbert, W. C. and Hogg, J. C. (1985). A re-assessment of the tricellular region of epithelial cell tight junctions in trachea of guinea pig. *Acta Anat. (Basel)* **122**, 35-38.

Watson, C. J., Rowland, M. and Warhurst, G. (2001). Functional modeling of tight junctions in intestinal cell monolayers using polyethylene glycol oligomers. *Am. J. Physiol. Cell Physiol.* **281**, C388-C397.

Wilcox, E. R., Burton, Q. L., Naz, S., Riazuddin, S., Smith, T. N., Ploplis, B., Belyantseva, I., Ben-Yosef, T., Liburd, N. A., Morell, R. J. et al. (2001). Mutations in the gene encoding tight junction claudin-14 cause autosomal recessive deafness DFNB29. *Cell* **104**, 165-172.

Yen, F. T., Masson, M., Clossais-Besnard, N., André, P., Grosset, J. M., Bougueleret, L., Dumas, J. B., Guerassimenko, O. and Bihain, B. E. (1999). Molecular cloning of a lipolysis-stimulated remnant receptor expressed in the liver. *J. Biol. Chem.* **274**, 13390-13398.